Environmental Science and Pollution Research (2018) 25:32466–32477
https://doi.org/10.1007/s11356-018-3119-3

RESEARCH ARTICLE

Enhancement of visible-light photocatalytic activities of $BiVO_4$ coupled with g-C_3N_4 prepared using different precursors

Peipei Cui[1] · Yun Hu[1,2] · Mengmeng Zheng[1] · Chaohai Wei[1,2]

Received: 8 April 2018 / Accepted: 31 August 2018 / Published online: 20 September 2018

Abstract

Graphitic-like carbon nitride (g-C_3N_4) photocatalyst was synthesized by a facile chemical pyrolysis method, which was built on the self-condensation of different precursors to generate g-C_3N_4, e.g., melamine, urea, and thiocarbamide. And the different precursors produced a great influence on the photocatalytic activities of g-C_3N_4. Heterojunctions of g-C_3N_4 and $BiVO_4$ were synthesized using a facile solvent evaporation method. The formation of $BiVO_4$/g-C_3N_4 composites were confirmed by XRD, FT-IR, SEM, XPS, and UV-Vis DRS. The photocatalytic activities for RhB degradation were evaluated under visible-light irradiation. The photocatalytic activity of g-C_3N_4 prepared by urea was higher than that of g-C_3N_4 prepared by melamine and thiocarbamide, which was attributed to its favorable dispersibility, larger specific surface area, and higher oxidation capacity. The heterojunction composites exhibited higher photocatalytic activity than pure g-C_3N_4 or $BiVO_4$. The results showed obvious removal efficiency for RhB, and the optimal sample with a $BiVO_4$ content of 10% exhibited higher efficiency than pure g-C_3N_4 and $BiVO_4$, and 10 wt%$BiVO_4$/CN-U showed the highest photocatalytic activity. The enhanced photocatalytic activity of $BiVO_4$/g-C_3N_4 composite can be attributed to the intimate coupling between the two host substrates, resulting in an efficient charge separation.

Keywords g-C_3N_4 · Precursor · $BiVO_4$ · Heterojunction · Photocatalytic oxidation

Introduction

Photocatalytic technology is an important method for dealing with environmental problems. Photocatalytic performance in semiconductor-based photocatalysis has received significant attention for the solar energy conversion (Li et al. 2007; Qiu et al. 2008; Yan et al. 2010; Wu et al. 2011) and environmental control (Molinari et al. 2013; Pei et al. 2013; Van Doorslaer et al. 2013; Oseghe et al. 2015; Lucchetti et al. 2017). Titanium dioxide (TiO_2) is the first artificial photocatalytic system for pollutant degradation, and it also is one of the best candidates for use in photovoltaic and photocatalytic devices due to its chemical stability, low cost, and nontoxicity (Chen and Mao 2007). However, TiO_2 can only be excited by ultraviolet (UV) light because of its large band gap, restricting its widespread use in many cases. Therefore, in order to make more efficient use of solar energy, many new potocatalysts that can be excited by visible light have been developed, such as $BiVO_4$ (Chen et al. 2017), Bi_2O_3(Shang et al. 2017), WO_3 (Gao et al. 2017), and g-C_3N_4 (Lan et al. 2016).

Carbon nitrides (C_3N_4) has attracted much attention since Wang discovered its photocatalytic property in 2009 (Wang et al. 2009). Graphitic carbon nitride (g-C_3N_4) as an old synthetic polymeric semiconductor with an indirect band gap of 2.7 eV, possesses excellent thermal, electrical, and optical characteristics (Zhang et al. 2013; Song et al. 2016; Suyana et al. 2017). g-C_3N_4 consists of carbon and nitrogen, which has the property of this abundant, geographically ubiquitous and simple synthetic method, and g-C_3N_4 can be synthesized

Responsible editor: Suresh Pillai

Electronic supplementary material The online version of this article (https://doi.org/10.1007/s11356-018-3119-3) contains supplementary material, which is available to authorized users.

✉ Yun Hu
huyun@scut.edu.cn

[1] Guangdong Provincial Key Laboratory of Atmospheric Environment and Pollution Control, School of Environment and Energy, South China University of Technology, Guangzhou 510006, People's Republic of China

[2] The Key Lab of Pollution Control and Ecosystem Restoration in Industry Clusters, Ministry of Education, Guangzhou 510006, People's Republic of China

with a simple thermal polymerization process by different precursors, e.g., melamine (Shi et al. 2014), thiocarbamide (Zhang et al. 2013), urea (Li et al. 2017), etc. However, the structure, element composition, and calcination process of the precursors can influence the morphology, crystalline form, and photocatalytic activity of samples, and until now, there are no research papers on the synthesis of g-C_3N_4 by different precursors to be connected with photocatalytic activity.

Meanwhile, g-C_3N_4 has several drawbacks, such as the poor visible harvesting efficiency and high photogenerated charge recombination rate, which have seriously limited its practical application (Caux et al. 2017; Zhang et al. 2017; Song et al. 2018). In recent years, the construction of heterostructure with matched conduction band and valence band has attracted many interests in improving the photocatalytic activity of composite semiconductor, e.g., SiO_2/Bi_2O_3/TiO_2 (Bai et al. 2017), g-C_3N_4/$Bi_2O_2CO_3$, and g-C_3N_4/BiOCl (Shan et al. 2016). Bismuth vanadate ($BiVO_4$) is a cheap, stable, and nontoxic pigment, and the narrow band gap about 2.4 eV prompts its meaningful applications in the subject of organic pollutants degradation under visible-light irradiation (Niu et al. 2015; Monfort et al. 2017). The modification of $BiVO_4$ with g-C_3N_4 has been reported for improving the photocatalytic activity compared with single component. Cheng et al. (2017) obtained g-C_3N_4/$BiVO_4$ by adding $BiVO_4$ to uniform urea solution before heat treatment for MB degradation. Jiang et al. (2017) synthesized all-solid-state RGO/g-C_3N_4/$BiVO_4$ by a hydrothermal method for the degradation of tetracycline. Wang et al. (2017) synthesized nanostructured g-C_3N_4/$BiVO_4$ by electrospinning for photoelectrochemical performance improvement. Compared with single component, the photocatalytic activity of the composite catalysts were significantly improved. However, they did not investigate the effect of g-C_3N_4 with different structures and physicochemical properties on the photocatalytic performance of the composites. Until now, little study has been reported about the effects of precursors on the intrinsic physicochemical properties of g-C_3N_4 under the same pyrolysis conditions. Hence, in this paper, we studied the composite materials of g-C_3N_4 synthesized by three different precursors and $BiVO_4$, as well as the difference of the photocatalytic activity.

In this work, we firstly developed a simple thermal polymerization process to synthesize g-C_3N_4 by three different precursors and discussed the impacts of different precursors on the morphologic structures and photocatalytic activities of the samples. We also used a facile solvent evaporation process to synthesize $BiVO_4$/g-C_3N_4 heterojunction photocatalyst for improving the photocatalytic activity. These composite catalysts were characterized via various techniques. Rhodamine B (RhB) was used as a model reactant to evaluate the photocatalytic activity of the prepared samples. In addition, the possible photocatalytic mechanism was proposed. This work was expected to be helpful for further development and application of g-C_3N_4-containing composites to the treatment of organic pollutants in water.

Experimental section

Materials

The following are the reagents used in this study: melamine ($C_3H_6N_6$, Aladdin, analytical reagent (AR)), urea (H_2NCONH_2, Tianjin Chemical Reagent Factory, AR), thiocarbamide (CN_2H_4S, Sinopharm Chemical Reagent Co, Ltd., AR), ammonium vanadate (Aladdin, AR), bismuth nitrate (Sinopharm Chemical Reagent Co, Ltd., AR), absolute ethanol(EtOH) (Sinopharm Chemical Reagent Co, Ltd., AR), sodium hydroxide (Aladdin, AR), nitric acid (Sinopharm Chemical Reagent Co, Ltd., AR), and rhodamine B (Tianjin Baishi Chemical Co, Ltd., AR). All other reagents used in this work were of AR grade.

Fabrication of materials

Preparation of g-C_3N_4 powder

Ten grams of melamine, urea, or thiocarbamide was placed in semiclosed crucibles, then calcined at 550 °C for 2 h with a heating rate of 15 °C/min, and after being naturally cooled to room temperature, g-C_3N_4 was obtained, which is named CN-M, CN-U, and CN-T, respectively.

Preparation of $BiVO_4$ powder

Five millimoles of $Bi(NO_3)_3{\cdot}5H_2O$ was dissolved in 10 mL aqueous solution of HNO_3 (4 M), meanwhile 5 mmol NH_4VO_3 was dissolved in 10 mL aqueous solution of NaOH (2 M), then mix the above two solutions to form a yellow transparent solution under vigorous stirring for 0.5 h, then NaOH solution (2 M) was added dropwise until pH = 7, followed by ultrasound treatment for 0.5 h. The synthetic mixture was then transferred to Teflon-lined autoclaves and maintained at 180 °C for 2 h. The autoclaves were then allowed to cool down to room temperature. Eventually, the synthetic solid was separated by centrifugation, and the conditions for the centrifugal separation were as follows: centrifugation time of 5 min, rotating speed at 5000 r/min, and then washed with water and ethanol three times and then dried at 80 °C in air.

Preparation of $BiVO_4$/g-C_3N_4 powder

One hundred milligrams of g-C_3N_4 was suspended in 20 mL of absolute ethanol. With constant vigorous stirring, X milligrams of $BiVO_4$ (X = 1, 5, 10, 20, 30, and 50) was added until

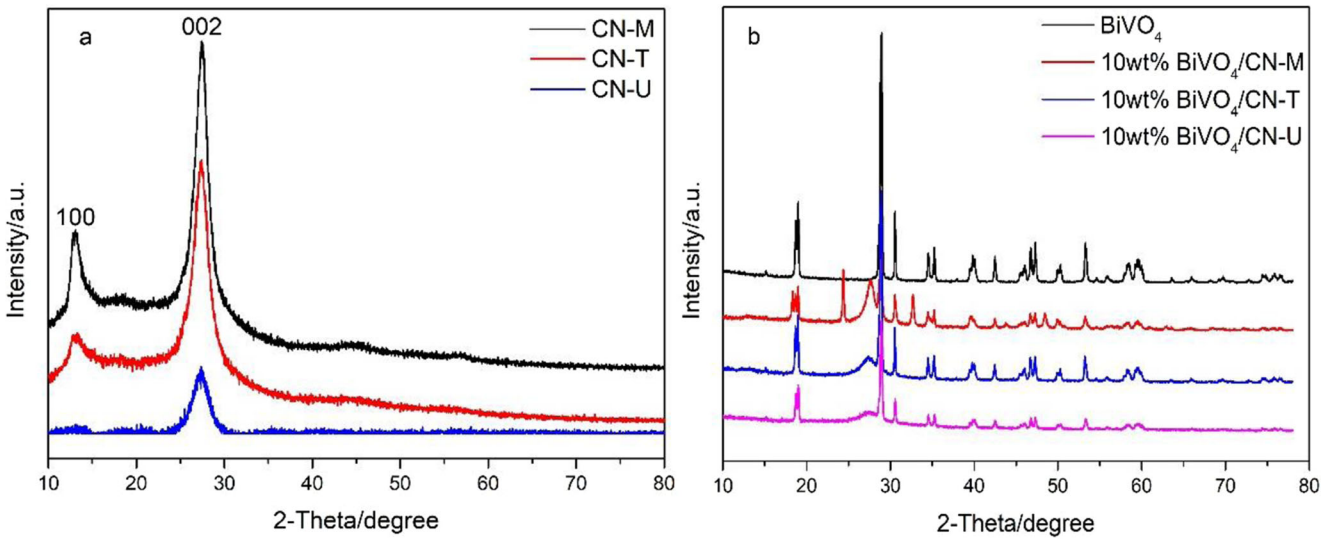

Fig. 1 XRD patterns of the prepared CN-M, CN-U, CN-T, $BiVO_4$, and $BiVO_4$/g-C_3N_4 photocatalysts

dried at room temperature, then a series of $BiVO_4$/g-C_3N_4 composites were obtained and denoted as *X* weight percent of $BiVO_4$/g-C_3N_4.

Characterizations

Powder X-ray diffraction (XRD) patterns of the catalysts were recorded with a D8 Advance diffractometer (Bruker AXS, Germany) with Cu Kα radiation (λ = 1.5418 Å). Fourier transform-infrared (FT-IR) was carried out on a Nicolet 6700 Fourier Transform IR spectrometer (Thermo, USA). The specific surface area was calculated using the Brunauer–Emmett–Teller (BET) method. Elemental analyses were performed on a Vario EL Cube elemental analyzer (Elementar, Germany). Scanning electron microscopy (SEM) was obtained using a Nova Nano SEM 430 field emission scanning electron microscope (FEI, USA). The UV-vis diffuse reflectance spectra (DRS) of the samples over a range of 250~800 nm was recorded by a UV-2550 powder UV-vis spectrophotometer (Shimadzu, Japan) with a $BaSO_4$ reference. X-ray

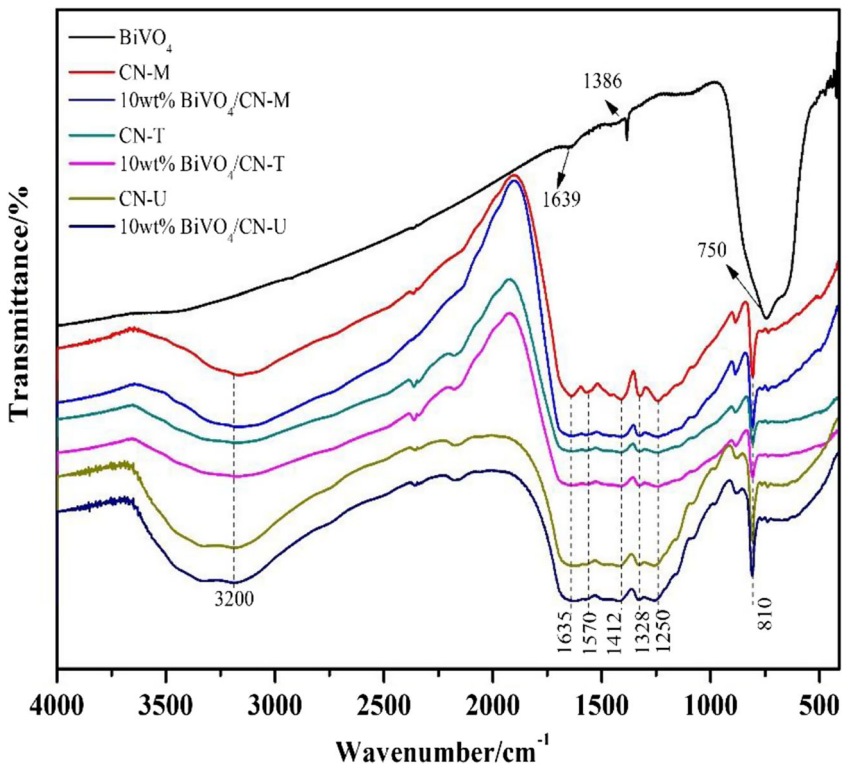

Fig. 2 FT-IR spectra of the prepared CN-M, CN-U, CN-T, $BiVO_4$, 10%$BiVO_4$/CN-M, 10% $BiVO_4$/CN-U, and 10% $BiVO_4$/CN-T samples

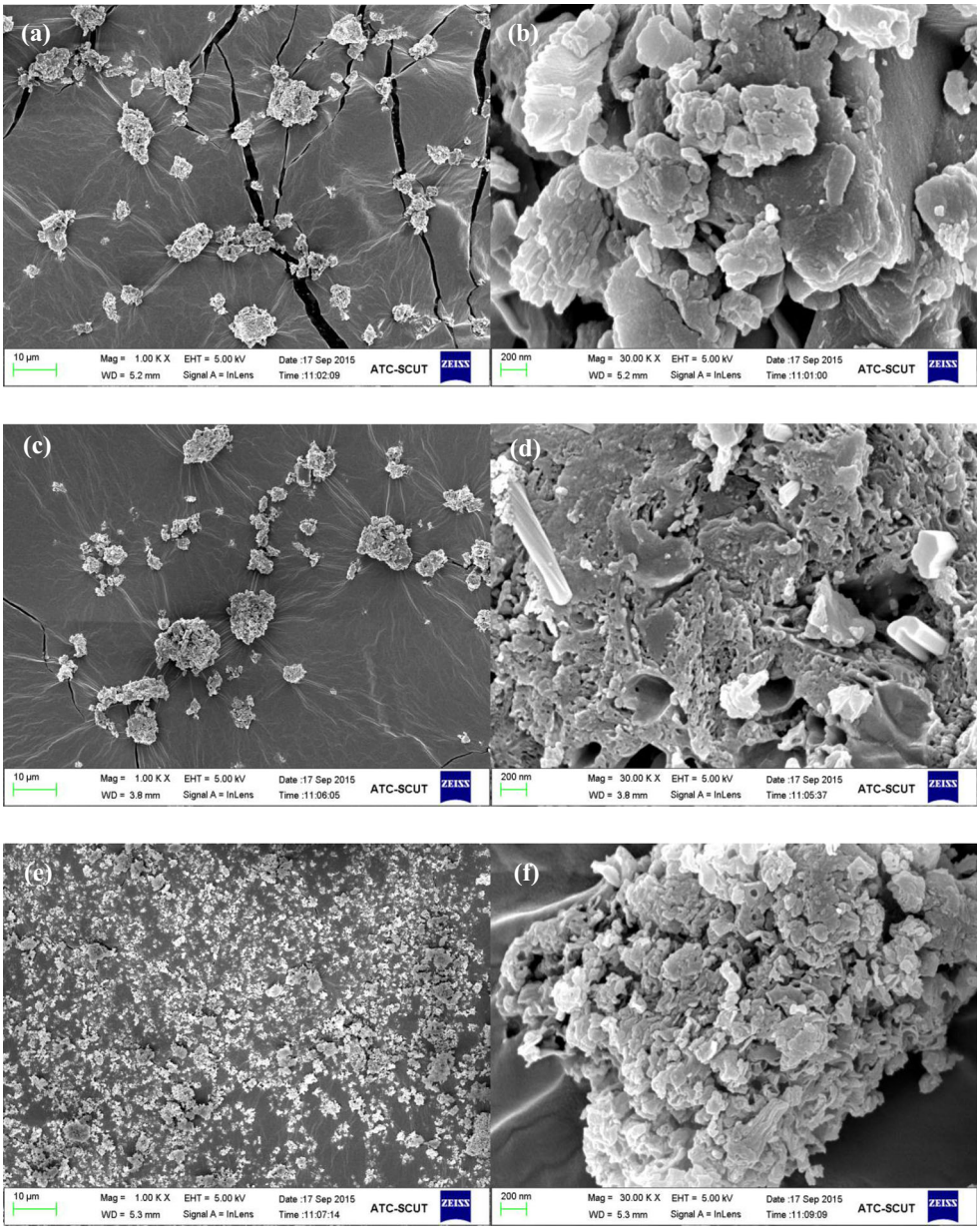

Fig. 3 SEM images of **a**, **b** CN-M, **c**, **d** CN-T, **e**, **f** CN-U, **g** $BiVO_4$, **h** $BiVO_4$/CN-M, **i** $BiVO_4$/CN-T, and **j** $BiVO_4$/CN-U

photoelectron spectroscopy (XPS) was performed on a Thermo Escalab 250Xi spectrometer (Thermo, USA) with a monochromatic Al Kα source. All the binding energies were referenced to the C1s peak at 284.8 eV of the surface adventitious carbon.

Evaluation of photocatalytic activity

RhB was used as a model reactant to evaluate the photocatalytic activity and self-cleaning property of the prepared samples. About 0.1 g sample was placed in 100 mL of 20 mg/L solution of RhB, and the suspension solution was stirred in the dark for 30 min to reach the adsorption equilibrium. Then, to further test the photocatalytic activity of the sample, a 500-W halogen lamp (1 mW/cm^2) with a cut-off filter ($\lambda > 420$ nm) was used as the visible-light source. The RhB concentration was analyzed by using a UV-vis spectrometer. The characteristic absorption peak of RhB at 554 nm was used to determine the extent of its degradation. The RhB removal ratio (η) was calculated as $\eta(\%) = (1–C/C_0) \times 100\%$, where C and C_0 are the concentrations of RhB after and before the reaction.

In the process of reusability and stability experiment, the used catalyst was firstly dipped in methanol for 12 h, washed with water for three times, and then dried at 80 °C in air for 12 h.

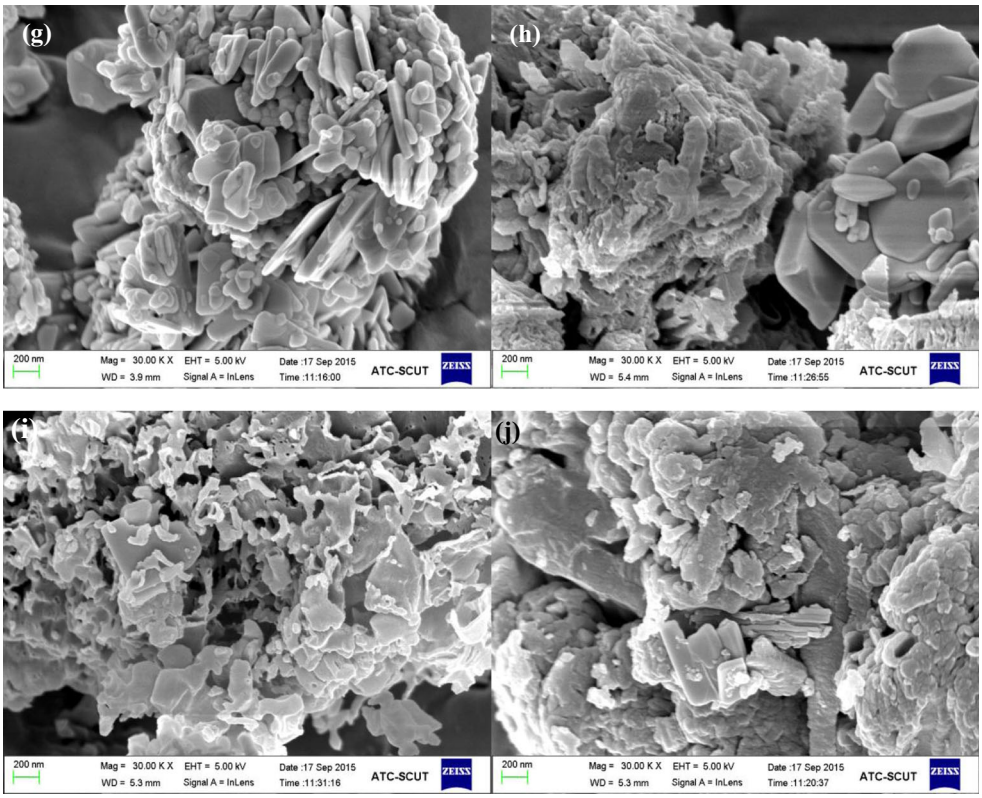

Fig. 3 (continued)

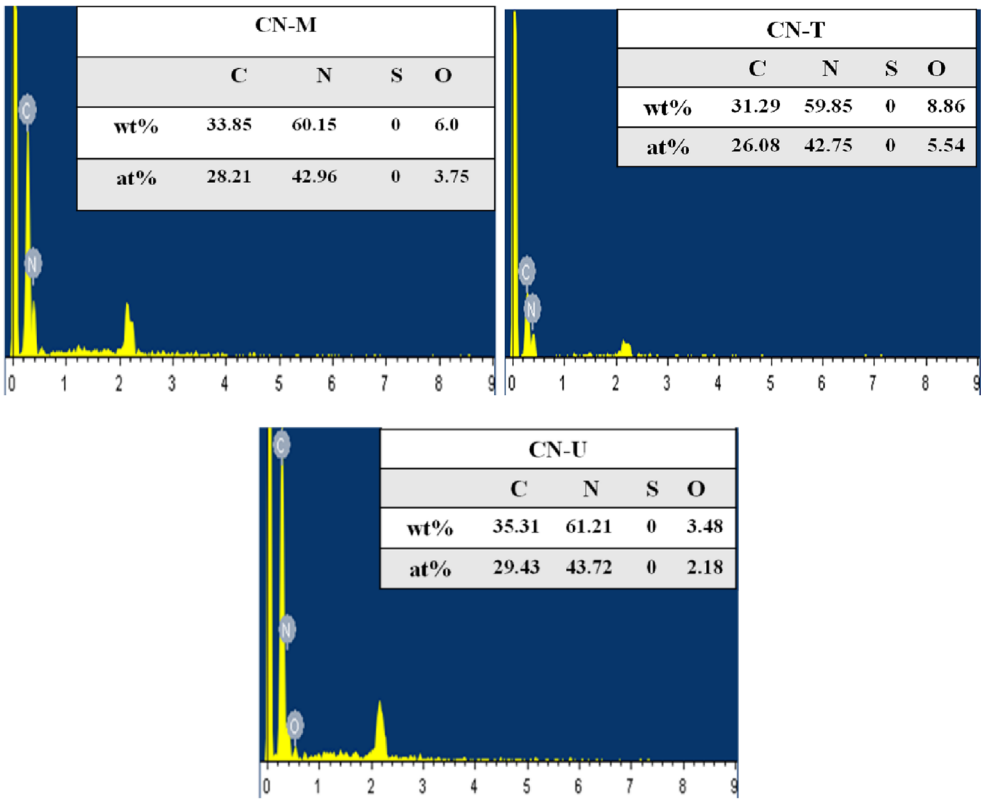

Fig. 4 Results of EDS analyses for CN-M, CN-T, and CN-U

Results and discussion

XRD analysis

The XRD patterns of CN-M, CN-T, CN-U, $BiVO_4$, and $BiVO_4$/g-C_3N_4 photocatalysts are shown in Fig. 1. Figure 1a shows the formation of the graphitic-like carbon nitride. CN-M, CN-T, and CN-U all have two characteristic peaks. The diffraction peak at 27.5° of g-C_3N_4 is a characteristic interlayer stacking reflection of conjugated aromatic systems, which can be indexed to (002) diffraction planes (JCPDS 87-1526); the corresponding crystalline interplanar spacing is 0.326 nm. The small peak at around 13.1° is indexed to (100) diffraction planes of g-C_3N_4, and the corresponding crystalline interplanar spacing is 0.675 nm (Dong et al. 2013). Figure 1a also shows that the diffraction intensity of (100) and (002) planes in CN-U are weaker than that in CN-M and CN-T, which may be because the CO_2 produced by C and O in urea during the calcination process inhibits the growth of the crystal surface, thus making the sample form structural defects. Meanwhile, the presence of S in thiocarbamide may also inhibit the growth of crystal surface. Therefore, the crystallization of g-C_3N_4 crystals prepared by three precursors is CN-M > CN-T > CN-U.

Figure 1b shows that the $BiVO_4$ has the same diffraction peaks as the composite samples (He et al. 2013), which may be because the diffraction peak intensity of g-C_3N_4 is weaker than that of $BiVO_4$. However, the composite samples have weak g-C_3N_4 peaks at 13.1° and 27.5°, indicating that the $BiVO_4$/g-C_3N_4 composites were successfully prepared.

FT-IR spectral analysis

Figure 2 shows the FT-IR spectra of the prepared samples. The spectra of the pure CN-M, CN-U, and CN-T have the characteristic peaks of g-C_3N_4, indicating that the g-C_3N_4 were successfully prepared by three different precursors. An absorption peak at ca. 810 and 1200~1650 cm^{-1} in the spectra of g-C_3N_4 can be assigned to the bending and stretching vibrations of C–N heterocycle, respectively (Li et al. 2014a, b), and a broad band at ca. 3200~3300 cm^{-1} in the spectra of all samples can be attributed to the stretching vibrations of O–H and N–H (Tian et al. 2011). Moreover, it can be observed that the intensity of absorption peak of CN-M at 1635 cm^{-1} is higher than that of CN-T and CN-U, which indicates that CN-M prepared with melamine has good crystallinity and structural integrity, which is consistent with the XRD results. For the pure $BiVO_4$, the absorption peaks at ca. 470 and 750 cm^{-1} can be assigned to the stretching vibrations of Bi–O and V–O, respectively (Tan et al. 2013), and a vibrational peak at ca. 1628 cm^{-1} can be attributed to the vibration of N–O, which comes from the reactant of NO_3^- in $Bi(NO_3)_3$ precursor (Wood and Glasser 2004). The characteristic peaks of g-C_3N_4 were found in the spectra of the $BiVO_4$/g-C_3N_4 composite catalysts, which further confirmed the formation of the composite catalysts.

Table 1 Elemental analysis results of CN-M, CN-T, and CN-U

Sample	N%	C%	H%	C/N molar ratio	S%
CN-M	59.74	33.42	1.89	0.653	0
CN-T	59.2	32.80	2.13	0.646	0
CN-U	61.80	35.50	2.76	0.670	0

Morphological analysis

SEM images of the samples are present in Fig. 3. It can be seen that the g-C_3N_4 prepared by three different precursors all possess obviously stratified structure. Figure 3a, c, and e shows that the g-C_3N_4 prepared by thiocarbamide is the most congregate; however, the g-C_3N_4 prepared by urea has a good dispersity and homogeneity. Meanwhile, the CN-U has smaller particles than CN-M and CN-T, perhaps it prompts that more reactive sites were exposed, which can facilitate access to pollutant and then promote catalytic activity. The CN-M prepared by melamine mostly presents sheets or blocks structure (Fig. 3b), and the size of nanosheets are about 200 nm. The CN-T prepared by thiocarbamide presents blocks with low porosity (Fig. 3d); however, the CN-U prepared by urea presents sheets with high porosity (Fig. 3f), which may be because the CO_2, NH_3, and H_2O vapor during the calcination process inhibited the growth of the crystal surface, consequently improving the specific surface area (Zhang et al. 2012). Thus, it can be seen that the different precursors have different molecular structures, and it plays an important role during the process of calcination to form g-C_3N_4.

Figure 3g shows the SEM image of pure $BiVO_4$, which indicated that pure $BiVO_4$ is reunited with thick sheets. The SEM images of $BiVO_4$/CN-M, $BiVO_4$/CN-T, and $BiVO_4$/CN-U composite catalysts are shown in Fig. 3h–j. The images

Table 2 BET analysis results of different catalysts

Sample	BET (m^2/g)
$BiVO_4$	2.31
CN-M	7.81
CN-T	26.72
CN-U	78.50
10 wt% $BiVO_4$/CN-M	7.31
10 wt% $BiVO_4$/CN-T	25.78
10 wt% $BiVO_4$/CN-U	75.56

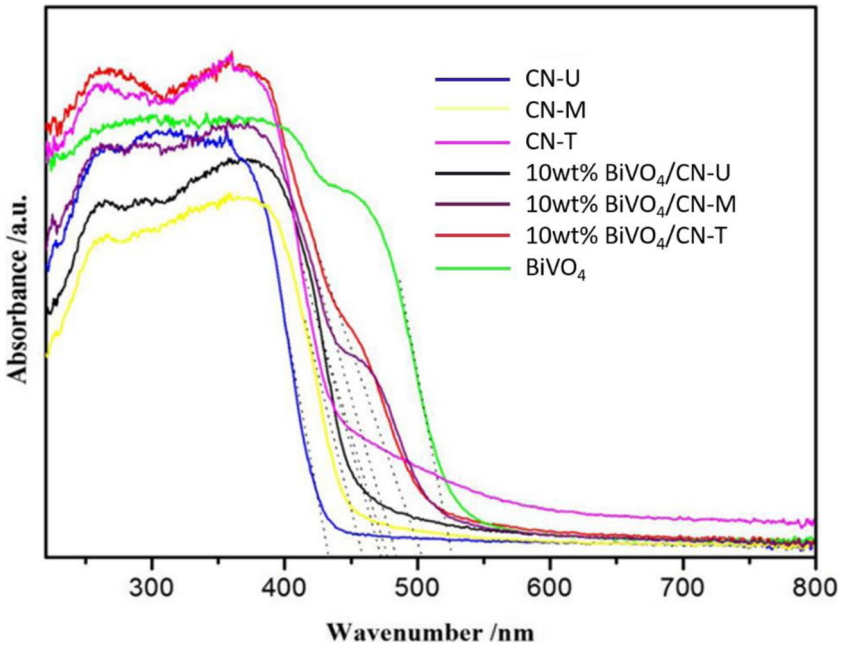

Fig. 5 The UV-vis diffuse reflectance spectra of g-C_3N_4, CN-M, CN-T, CN-U, and 10 wt% $BiVO_4$/g-C_3N_4

exhibit that $BiVO_4$ sheet closely contacts with block g-C_3N_4, thus it is beneficial for the spatially separated catalysts to drive electrons and holes, and it is beneficial to improve the photocatalytic activity eventually.

EDS and elemental analysis

Figure 4 shows the element composition of the g-C_3N_4. The samples mainly included are C, N, and O elements. The molar ratio of C/N is 0.657, 0.611, and 0.673 that corresponds to CN-M, CN-T, and CN-U, respectively, which is consistent with the theoretical value (Wang et al. 2009). The result indicated that the g-C_3N_4 was successfully prepared by three different precursors, and the sulfur in thiocarbamide was removed completely by calcination.

In order to further study the element composition of g-C_3N_4 which were prepared by three different precursors, the elemental analyses were carried out. Table 1 shows that the molar ratio of C/N in CN-M, CN-T, and CN-U are 0.653, 0.646, and 0.670, respectively, which are lower than the theoretical value (0.75), due to the formation of amino group from thermal condensation at the calcination process. It can

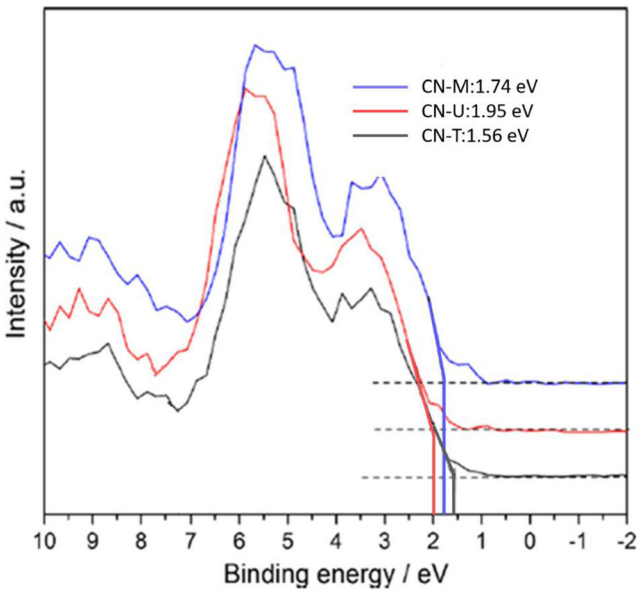

Fig. 6 VB XPS spectra of g-C_3N_4 prepared using different precursors

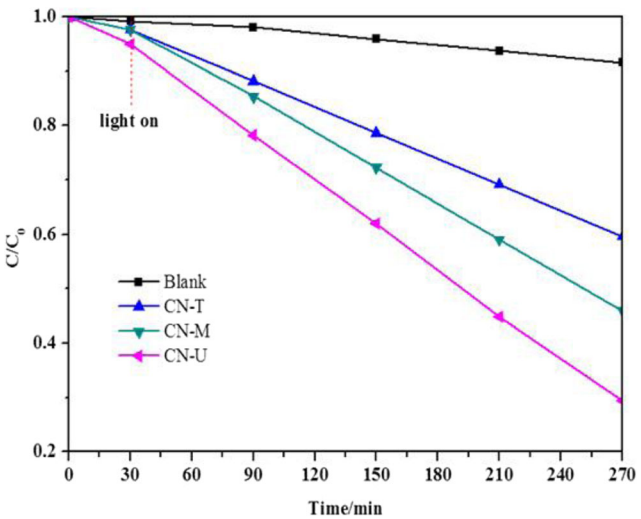

Fig. 7 The photocatalytic degradation of RhB by g-C_3N_4 prepared using different precursors under visible light

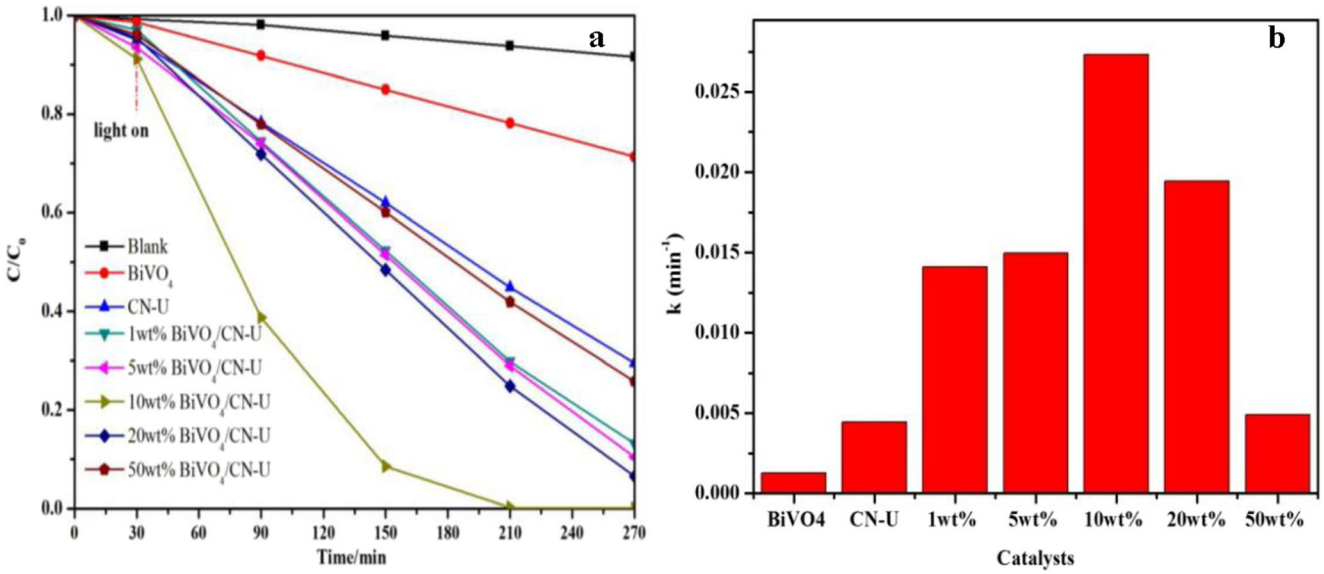

Fig. 8 **a** The photocatalytic degradation of RhB by different catalysts under visible light: $BiVO_4$/CN-U composite photocatalyst with different $BiVO_4$ content; **b** the comparison of rate constant K. (C_{RhB} = 20 mg/L, $M_{BiVO4/CN-U}$ = 0.1 g, pH = 7)

also be proven by the results of the FT-IR spectral analyses, in which the result showed the existence of amino group.

BET analysis

Table 2 displays the specific surface area of the samples. Compared with CN-M and CN-T, the CN-U shows a larger specific surface area of 78.5 m^2/g, which may be because the CO_2 produced during the calcination process made the sample form more structural defects, thus increasing the specific surface area. The pure $BiVO_4$ is reunited with thick sheets so that it has a small specific surface area of 2.31 m^2/g. Compared with the pure photocatalysts, the specific surface areas of the 10% $BiVO_4$/g-C_3N_4 composites showed no change, indicating that the loading of $BiVO_4$ has no influence on the specific surface area.

UV-vis diffuse reflectance spectra and VB XPS spectra analysis

UV-vis diffuse reflectance spectra measurement is employed to characterize the optical properties of the samples. As shown

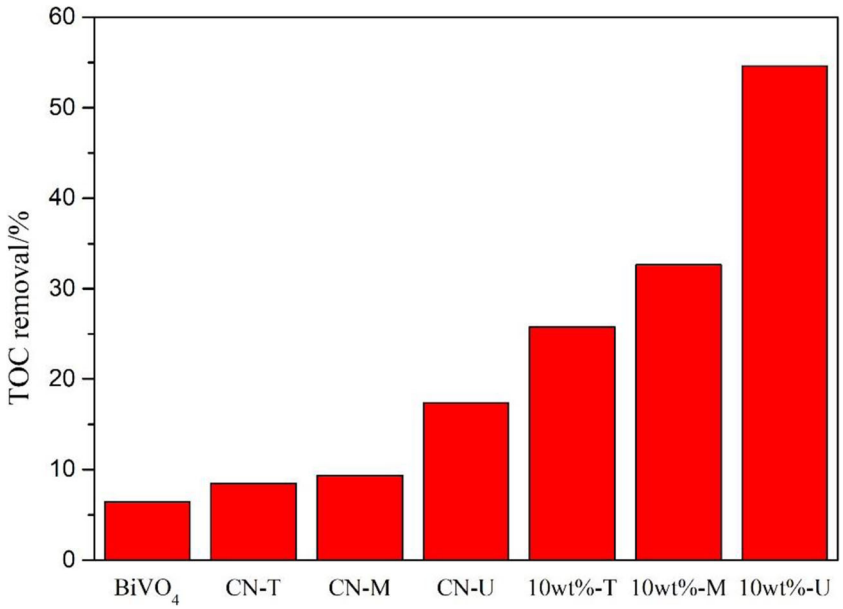

Fig. 9 Removal rate of $BiVO_4$/g-C_3N_4 composite photocatalysts for TOC ($M_{BiVO4/g-C3N4}$ = 0.1 g, pH = 7)

in Fig. 5, all the samples have obvious visible-light absorption, and the optical adsorption edges of CN-M, CN-T, and CN-U are present at ca. 456, 475, and 437 nm, corresponding to 2.72, 2.61, and 2.84 eV of the band gap, respectively. CN-U has broader band gap so that it has stronger oxidizability of pollutants than CN-M and CN-T. CN-T shows the stronger absorption intensities compared with CN-M and CN-U in the visible region due to the different degrees of condensation of the precursors during the condensation process (Dong et al. 2013). The optical absorption edge of pure $BiVO_4$ is present in ca. 524 nm, corresponding to 2.37 eV of the band gap. Compared with the pure g-C_3N_4, all composite samples show a certain extent of red shift, corresponding to the high utilization of the visible light, and further indicating that the $BiVO_4$/g-C_3N_4 composite photocatalysts have been successfully prepared.

Figure 6 shows the valence band (VB) XPS spectra of different g-C_3N_4 catalysts; the maximal valence bands of CN-T, CN-M, and CN-U are present at 1.56, 1.74, and 1.95 eV, respectively. Compared with CN-T and CN-M, CN-U has more positive valence band. With the UV-vis diffuse reflectance spectra, it can be calculated that the conduction bands of CN-T, CN-M, and CN-U are present at − 1.05, − 0.98, and − 0.89 eV, respectively. The conduction band can be calculated by the band gap and the valence band ($E_C = E_B - E_g$, where E_C is conduction band, E_B is valence band, and E_g is band gap).

Photocatalytic property of samples

Photocatalytic degradation of RhB was carried out to determine the photocatalytic properties of the prepared samples. Figure 7 shows the time course of RhB removal efficiency over the three samples. It can be seen that all the samples have little adsorption for RhB, and the RhB degradation efficiency on CN-T, CN-M, and CN-U are 42, 55, and 71% after visible-light irradiation for 240 min. In our work, the energy generated by the halogen lamp ($\lambda > 420$ nm) is enough to stimulate the separation of electrons and holes from all the catalysts. The CN-U prepared by urea has the largest band gap, so it has stronger oxidizability than that prepared by melamine and thiocarbamide. Moreover, the different precursors used in preparation of g-C_3N_4 made the differences in the morphology, structure and photochemical property of the three g-C_3N_4 samples. Compared with the g-C_3N_4 prepared by melamine and thiocarbamide, the catalyst prepared by urea showed better dispersity and homogeneity, stronger oxidizability, as well as higher specific surface area, which facilitated the dispersion of $BiVO_4$ and provided more active sites for photocatalytic reaction (Zhang et al. 2013; Suyana et al. 2017), resulting in higher photocatalytic activity.

In order to further improve the photocatalytic efficiency of the prepared g-C_3N_4 catalysts, $BiVO_4$ was combined with g-C_3N_4 to form composite photocatalysts with heterojunction. Figure 8a shows the photocatalytic degradation efficiency of RhB on $BiVO_4$/CN-U composite photocatalyst with different $BiVO_4$ contents. Compared with the pure $BiVO_4$ or CN-U, all $BiVO_4$/CN-U composites exhibit higher photocatalytic activity, and when the mass percentage of $BiVO_4$ is 10 wt%, it can reach the highest photocatalytic activity and the removal efficiency of RhB reaches 100% within 210 min. The addition of $BiVO_4$ contributes the separation of negative electrons and positive holes, but with the further increase of the $BiVO_4$ content, the excess $BiVO_4$ as recombination center of the photogenerated carriers against the separation of electrons and holes, resulting in the decrease in photocatalytic activity. Therefore, enhancing the separation rate of photogenerated electrons and holes is a crucial method for improving the

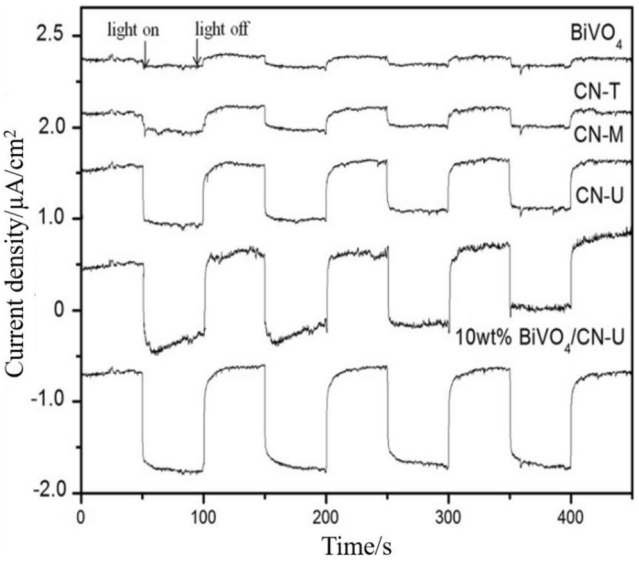

Fig. 10 The photocurrent of the samples

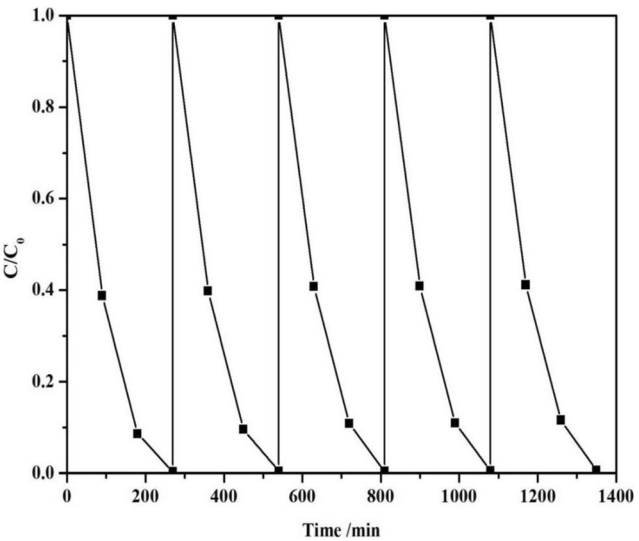

Fig. 11 The stability investigation of 10 wt% $BiVO_4$/CN-U composite photocatalyst. ($M_{BiVO4/CN-U} = 0.1$ g, pH = 7)

photocatalytic activity. In addition, Fig. S1 shows the linear relationship between $\ln(C/C_0)$ and irradiation time, indicating that the photocatalytic degradation of RhB over the as-prepared catalysts belongs to the first-order kinetic relation. Meanwhile, Fig. 8b displays the composite photocatalyst of 10 wt% $BiVO_4$/CN-U that has the highest photocatalytic activity, and the reaction rate constant for 10 wt% $BiVO_4$/CN-U is 11.2 and 5.3 times as that of $BiVO_4$ and CN-U, respectively. The results indicated that the adding of $BiVO_4$ can enhance the separation rate of photogenerated charge carriers, thus remarkably improving the photocatalytic activity.

Fig. S2a and S2b shows the photocatalytic degradation of RhB by $BiVO_4$/CN-M and $BiVO_4$/CN-T composites with different $BiVO_4$ contents. Compared with the pure $BiVO_4$, CN-M, or CN-T, all $BiVO_4$/CN-M and $BiVO_4$/CN-T composites showed higher photocatalytic activities, and the highest activity was achieved at 10 wt% of $BiVO_4$ loading. This is consistent with the result of $BiVO_4$/CN-U. These results indicated that due to the combination of $BiVO_4$ with g-C_3N_4 prepared by different precursors, the interfacial charge transfer between the two semiconductors inhibited the recombination of charge carriers, thereby improving the photocatalytic activity significantly.

In order to evaluate the mineralization degree of RhB, the total organic carbon (TOC) removal efficiency of RhB in different samples were detected (Fig. 9). An apparent decrease in the amount of TOC was observed for the different samples, the mineralization rate of RhB on the composite catalysts was higher than that on the single catalyst, and 10 wt% $BiVO_4$/CN-U has the highest mineralization rate reaching 54.6%.

Photocurrent of the samples

The photocurrent of the photocatalysts are shown in Fig. 10. It can be seen that CN-U showed higher separating rate of carriers than CN-T and CN-M, thereby showing higher photocatalytic activity. The composite photocatalyst of 10 wt% $BiVO_4$/CN-U has an advantageous density of photocurrent over the sum of that of CN-U and $BiVO_4$, indicating that the combination of $BiVO_4$ and CN-U immensely promotes the separation of photogenerated electrons and holes, thus remarkably improving the photocatalytic activity.

Reusability and stability of the 10-wt% $BiVO_4$/CN-U

Figure 11 shows recycled results of 10 wt% $BiVO_4$/CN-U. The 10-wt% $BiVO_4$/CN-U shows high stability. After five reaction cycles, the removal efficiency of RhB was still maintained at 100% compared with the performance of fresh photocatalysts, which shows that the $BiVO_4$/CN-U composite could be a stable and excellent photocatalyst for RhB removal.

Possible mechanism of $BiVO_4$/CN-U

According to the results of UV-vis and XPS, we can know that the conduction and valence band (CB/VB) of CN-U and $BiVO_4$ are − 0.89 eV/1.95 eV and 0 eV/2.37 eV. Therefore, the CB and VB electrochemical potentials of CN-U and $BiVO_4$ as well as the probable charge separation process of $BiVO_4$/CN-U composite are illustrated in Fig. 12. It can be seen that the CN-U and $BiVO_4$ have different energy bands, so it benefits the interfacial transfer of photon-generated carriers. Moreover, *n*–*n* heterojunction is constituted by *n*-type CN-U with *n*-type $BiVO_4$, forming electric field (Li et al. 2014a, b; Cheng et al. 2017). The electrons on the valence band of CN-U and $BiVO_4$ can be excited by the high-energy photon under the visible-light irradiation. Based on the principle of charge transfer between the interfaces, the holes on the valence band of $BiVO_4$ can easily transfer to the valence band

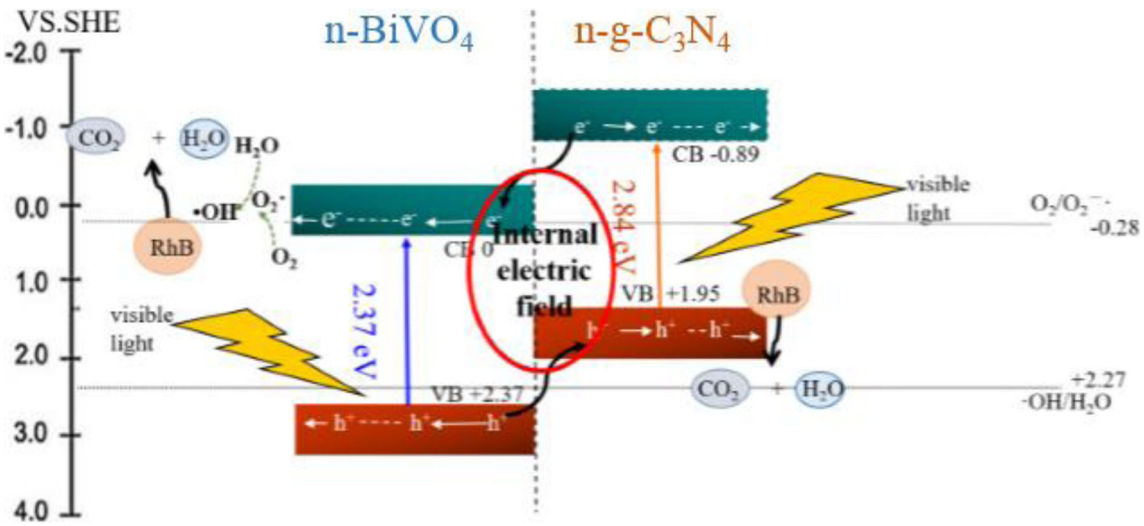

Fig. 12 The photocatalytic degradation mechanism of RhB over $BiVO_4$/g-C_3N_4

of CN-U, and the electrons on the conduction band of CN-U can easily transfer to the conduction band of $BiVO_4$, therefore the possibility of electron-hole recombination was reduced. The electrons in the conduction band of $BiVO_4$ can participate in the reactions assisted by O_2 dissolved in water, consequently, to generate H_2O_2 and ·OH, which can be used to oxidize RhB to form CO_2 and H_2O. And the holes in the valence band of CN-U can oxidize RhB directly to form CO_2 and H_2O.

Conclusions

In conclusion, we firstly developed a simple thermal polymerization process to synthesize g-C_3N_4 by three different precursors and utilized a facile solvent evaporation process to synthesize $BiVO_4$/g-C_3N_4 composite catalysts. Compared with the g-C_3N_4, CN-T, and CN-M, prepared with thiocarbamide and melamine, CN-U prepared with urea had a higher photocatalytic activity under visible light since CN-U had higher homogeneity, larger specific surface area, higher oxidation capacity, and higher separation rate of charge carriers. Moreover, the $BiVO_4$/g-C_3N_4 composites had higher photocatalytic activity than the pure $BiVO_4$ or g-C_3N_4, and it reached the highest activity when the $BiVO_4$ content was 10 wt%. Such improvement was attributed to the successful inhibition of the recombination of photogenerated electrons and holes by the composite photocatalysts with appropriate combination ratio.

Funding information This work was supported by the National Natural Science Foundation of China (21577039, 21777047, 21277051), Science and Technology Planning Project of Guangdong Province, China (2015A020215004), and Scientific Research Project of Guangzhou City (201804020026).

References

Bai ZG, Hu Y, Yan SQ, Shan WJ, Wei CH (2017) Preparation of mesoporous SiO_2/Bi_2O_3/TiO_2 superhydrophilic thin films and their surface self-cleaning properties. RSC Adv 7:1966–1974

Caux M, Fina F, Irvine JT, Idriss H, Howe R (2017) Impact of the annealing temperature on Pt/g-C_3N_4 structure, activity and selectivity between photodegradation and water splitting. Catal Today 287: 182–188

Chen X, Mao S (2007) Titanium dioxide nanomaterials: synthesis, properties, modifications, and applications. Chem Rev 107:2891–2959

Chen F, Yang Q, Wang Y, Zhao J, Wang D, Li X, Zeng G (2017) Novel ternary heterojunction photcocatalyst of Ag nanoparticles and g-C_3N_4 nanosheets co-modified $BiVO_4$ for wider spectrum visible-light photocatalytic degradation of refractory pollutant. Appl Catal B Environ 205:133–147

Cheng J, Yan XL, Mo QH, Liu BT, Wang J, Yang X, Li L (2017) Facile synthesis of g-C_3N_4/$BiVO_4$ heterojunctions with enhanced visible light photocatalytic performance. Ceram Int 43:301–307

Dong F, Zhao ZW, Xiong T, Ni ZL, Zhang WD, Sun YJ, Ho WK (2013) In situ construction of g-C_3N_4/g-C_3N_4 metal-free heterojunction for enhanced visible-light photocatalysis. ACS Appl Mater Interfaces 5(21):11392–11401

Gao H, Zhang P, Zhao J, Zhang Y, Hu J, Shao G (2017) Plasmon enhancement on photocatalytic hydrogen production over the Z-scheme photosynthetic heterojunction system. Appl Catal B Environ 210:297–305

He Z, Shi Y, Gao C, Wen L, Chen J, Song S (2013) BiOCl/$BiVO_4$ p–n heterojunction with enhanced photocatalytic activity under visible-light irradiation. J Phys Chem C 118(1):389–398

Jiang DL, Xiao P, Shao LQ, Li D, Chen M (2017) RGO-promoted all-solid-state g-C_3N_4/$BiVO_4$ Z-scheme heterostructure with enhanced photocatalytic activity toward the degradation of antibiotics. Ind Eng Chem Res 56:8823–8832

Lan ZA, Zhang G, Wang X (2016) A facile synthesis of Br-modified g-C_3N_4 semiconductors for photoredox water splitting. Appl Catal B Environ 192:116–125

Li H, Bian Z, Zhu J, Zhang D, Li G, Huo Y, Lu Y (2007) Mesoporous titania spheres with tunable chamber stucture and enhanced photocatalytic activity. J Am Chem Soc 129(27):8406–8407

Li H, Liu J, Hou W, Du N, Zhang R, Tao X (2014a) Synthesis and characterization of g-C_3N_4/Bi_2MoO_6 heterojunctions with enhanced visible light photocatalytic activity. Appl Catal B Environ 160:89–97

Li CJ, Wang SP, Wang T, Wei YJ, Zhang P (2014b) Monoclinic porous $BiVO_4$ networks decorated by discrete g-C_3N_4 nano-islands with tunable coverage for highly efficient photocatalysis. Small 10(14): 2782–2782

Li C, Du Y, Wang D, Yin S, Tu W, Chen Z, Xu R (2017) Unique P-Co-N surface bonding states constructed on g-C_3N_4 nanosheets for drastically enhanced photocatalytic activity of H_2 evolution. Adv Funct Mater 27:1604328

Lucchetti R, Siciliano A, Clarizia L, Russo D, Di Somma I, Di Natale F, Marotta R (2017) Sacrificial photocatalysis: removal of nitrate and hydrogen production by nano-copper-loaded P25 titania. A kinetic and ecotoxicological assessment. Environ Sci Pollut Res 24(6): 5898–5907

Molinari A, Argazzi R, Maldotti A (2013) Photocatalysis with $Na_4W_{10}O_{32}$ in water system: formation and reactivity of OH radicals. J Mol Catal A Chem 372:23–28

Monfort O, Sfaelou S, Satrapinskyy L, Plecenik T, Roch T, Plesch G, Lianos P (2017) Comparative study between pristine and Nb-modified $BiVO_4$ films employed for photoelectrocatalytic production of H_2 by water splitting and for photocatalytic degradation of organic pollutants under simulated solar light. Catal Today 280:51–57

Niu M, Zhu R, Tian F, Song K, Cao G, Ouyang F (2015) The effects of precursors and loading of carbon on the photocatalytic activity of C–$BiVO_4$ for the degradation of high concentrations of phenol under visible light irradiation. Catal Today 258:585–594

Oseghe EO, Ndungu PG, Jonnalagadda SB (2015) Synthesis of mesoporous Mn/TiO_2 nanocomposites and investigating the photocatalytic properties in aqueous systems. Environ Sci Pollut Res 22(1):211–222

Pei LZ, Wang S, Jiang YX, Xie YK, Li Y, Guo YH (2013) Single crystalline Sr germanate nanowires and their photocatalytic performance for the degradation of methyl blue. CrystEngComm 15(38):7815–7823

Qiu X, Li L, Zheng J, Liu J, Sun X, Li G (2008) Origin of the enhanced photocatalytic activities of semiconductors: a case study of ZnO doped with Mg^{2+}. J Phys Chem C 112(32):12242–12248

Shan WJ, Hu Y, Bai ZG, Zheng MM, Wei CH (2016) In situ preparation of g-C_3N_4/bismuth-based oxide nanocomposites with enhanced photocatalytic activity. Appl Catal B Environ 188:1–12

Shang Z, Sun M, Chang S, Che X, Cao X, Wang L, Lu G (2017) Activity and stability of Co_3O_4-based catalysts for soot oxidation: the enhanced effect of Bi_2O_3 on activation and transfer of oxygen. Appl Catal B Environ 209:33–44

Shi H, Chen G, Zhang C, Zou Z (2014) Polymeric g-C_3N_4 coupled with $NaNbO_3$ nanowires toward enhanced photocatalytic reduction of CO_2 into renewable fuel. ACS Catal 4(10):3637–3643

Song X, Hu Y, Zheng MM, Wei CH (2016) Solvent-free in situ synthesis of g-C_3N_4/{001}TiO_2 composite with enhanced UV-and visible-light photocatalytic activity for NO oxidation. Appl Catal B Environ 182:587–597

Song C, Fan M, Shi W, Wang W (2018) High-performance for hydrogen evolution and pollutant degradation of reduced graphene oxide/two-phase g-C_3N_4 heterojunction photocatalysts. Environ Sci Pollut Res 25:14486–14498

Suyana P, Priyanka G, Nair BN, Abdul APM, Krishna GKW (2017) Role of precursors on the photophysical properties of carbon nitride and its application for antibiotic degradation. Environ Sci Pollut Res Int 24(9):8609–8618

Tan G, Zhang L, Ren H, Wei S, Huang J, Xia A (2013) Effects of pH on the hierarchical structures and photocatalytic performance of $BiVO_4$ powders prepared via the microwave hydrothermal method. ACS Appl Mater Interfaces 5(11):5186–5193

Tian G, Chen Y, Zhou W, Pan K, Dong Y, Tian C, Fu H (2011) Facile solvothermal synthesis of hierarchical flower-like $BiMoO_6$ hollow spheres as high performance visible-light driven photocatalysts. J Mater Chem 21(3):887–892

Van Doorslaer X, Demeestere K, Heynderickx PM, Caussyn M, Van Langenhove H, Devlieghere F, Dewulf J (2013) Heterogeneous photocatalysis of moxifloxacin: identification of degradation products and determination of residual antibacterial activity. Appl Catal B Environ 138:333–341

Wang X, Maeda K, Thomas A, Takanabe K, Xin G, Carlsson JM, Antonietti M (2009) A metal-free polymeric photocatalyst for hydrogen production from water under visible light. Nat Mater 8(1): 76–80

Wang Y, Sun JY, Li J, Zhao X (2017) Electrospinning preparation of nanostructured g-C_3N_4/$BiVO_4$ composite films with an enhanced photoelectrochemical performance. Langmuir 33:4694–4701

Wood P, Glasser FP (2004) Preparation and properties of pigmentary grade $BiVO_4$ precipitated from aqueous solution. Ceram Int 30(6): 875–882

Wu W, Zhang SF, Ren F, Xiao XH, Zhou J, Jiang CZ (2011) Controlled synthesis of magnetic iron oxides@SnO_2 quasi-hollow core–shell heterostructures: formation mechanism, and enhanced photocatalytic activity. Nano 3:4676–4684

Yan SC, Lv SB, Li ZS, Zou ZG (2010) Organic–inorganic composite photocatalyst of g-C_3N_4 and TaON with improved visible light photocatalytic activities. Dalton Trans 39(6):1488–1491

Zhang GG, Zhang JS, Zhang MW, Wang XC (2012) Polycondensation of thiourea into carbon nitride semiconductors as visible light photocatalysts. J Mater Chem 22:8083–8091

Zhang J, Wang Y, Jin J, Zhang J, Lin Z, Huang F, Yu J (2013) Efficient visible-light photocatalytic hydrogen evolution and enhanced photostability of core/shell CdS/g-C_3N_4 nanowires. ACS Appl Mater Interfaces 5(20):10317–10324

Zhang Q, Xu B, Yuan S, Zhang M, Ohno T (2017) Improving g-C_3N_4 photocatalytic performance by hybridizing with $Bi_2O_2CO_3$ nanosheets. Catal Today 284:27–36